

# Carboxy Terminus Splice Variation Alters ClC Channel Gating and Extracellular Cysteine Reactivity

Liping He,\* Jerod Denton,\* Keith Nehrke,<sup>†</sup> and Kevin Strange\*

\*Departments of Anesthesiology, Molecular Physiology and Biophysics, and Pharmacology, Vanderbilt University Medical Center, Nashville, Tennessee 37232; and <sup>†</sup>Department of Medicine, Division of Nephrology, University of Rochester Medical Center, Rochester, New York 14642

**ABSTRACT** CLH-3a and CLH-3b are *Caenorhabditis elegans* ClC channel splice variants that exhibit striking differences in voltage, Cl<sup>-</sup>, and H<sup>+</sup> sensitivity. The major primary structure differences between the channels include a 71 amino acid CLH-3a N-terminal extension and a 270 amino acid extension of the CLH-3b C-terminus. Deletion of the CLH-3a N-terminus or generation of a CLH-3a/b chimera has no effect on channel gating. In contrast, deletion of a 169 amino acid C-terminal CLH-3b splice insert or deletion of the last 11 amino acids of cystathionine- $\beta$ -synthase domain 1 gives rise to functional properties identical to those of CLH-3a. Voltage-, Cl<sup>-</sup>, and H<sup>+</sup>-dependent gating of both channels are lost when their glutamate gates are mutated to alanine. Glutamate gate cysteine mutants exhibit similar degrees of inhibition by MTSET, but the inhibition time constant of CLH-3b is sevenfold greater than that of CLH-3a. Differences in MTSET inhibition are reversed by deletion of the same cytoplasmic C-terminal regions that alter CLH-3b gating. Our results indicate that splice variation of the CLH-3b cytoplasmic C-terminus alters extracellular structure and suggest that differences in the conformation of the outer pore vestibule and associated glutamate gate may account for differences in CLH-3a and CLH-3b gating.

## INTRODUCTION

The first member of the ClC superfamily of voltage-gated Cl<sup>-</sup> channels was identified in 1990 by Jentsch and co-workers (1). ClC-encoding genes have since been found in plants, fungi, animals, and bacteria. In animals, ClC channels play key roles in diverse and fundamental physiological processes including regulation of skeletal muscle membrane excitability and cytoplasmic Cl<sup>-</sup> levels, transepithelial Cl<sup>-</sup> transport, and acidification of intracellular vesicles. Nine ClC genes have been identified in mammals, and mutations in five of these are associated with inherited muscle, bone, kidney, and neurological diseases (2,3).

Recent x-ray crystallographic studies of bacterial ClCs indicate that the proteins form homodimers and that an independently gated pore is present in each subunit (4,5) as originally postulated by Miller and co-workers (6,7). Bacterial ClC monomers are composed of short intracellular amino (N)- and carboxyl (C)-termini and 18  $\alpha$ -helical domains (termed A–R; Fig. 1), 17 of which are intramembrane (5). Structure/function analysis of vertebrate ClC channels indicates that the overall membrane and pore structure of ClCs is likely conserved in prokaryotes and eukaryotes (e.g., 8–10). However, a major and important structural difference between the ClC proteins of these two groups of organisms is the presence in eukaryotic ClCs of a large cytoplasmic C-terminus containing two highly conserved cystathionine- $\beta$ -synthase or CBS domains (11). Dutzler et al. (5) dem-

onstrated that the most C-terminal  $\alpha$ -helix (helix R) of the *Salmonella enterica* ClC participates in Cl<sup>-</sup> coordination within the selectivity filter. They postulated that in eukaryotes the attachment of helix R to the cytoplasmic C-terminus could provide a structural basis for regulating channel gating.

*clh-3* is a *Caenorhabditis elegans* ClC-encoding gene (12,13). Two *clh-3* encoded splice variants have been identified, CLH-3a and CLH-3b (12–14). These proteins have identical intramembrane domains but differ significantly in their cytoplasmic N- and C-termini (Fig. 1). CLH-3b is expressed in the worm oocyte and is activated by serine/threonine dephosphorylation during cell swelling and oocyte meiotic maturation (15–17). Meiotic maturation-induced channel activation functions to synchronize oocyte cell cycle progression with ovulation and fertilization (16,18).

We recently carried out extensive functional characterization of CLH-3a and CLH-3b expressed heterologously in HEK293 cells (14). The two channels differ strikingly in their biophysical properties. CLH-3a requires stronger hyperpolarization for activation than CLH-3b. Depolarizing conditioning voltages dramatically increase CLH-3a current amplitude and induce a slow inactivation process at hyperpolarized voltages but have no effect on CLH-3b activity. CLH-3a also exhibits significantly greater sensitivity to extracellular Cl<sup>-</sup> and H<sup>+</sup>.

The purpose of this investigation was to test the hypothesis that alternative splicing of the cytoplasmic C-terminus gives rise to the gating properties of CLH-3a and CLH-3b. Deletion of the unique CLH-3a N-terminus or generation of a CLH-3a/b chimera has no effect on channel voltage, Cl<sup>-</sup>, or H<sup>+</sup> sensitivity. In contrast, deletion of a 169 amino acid

Submitted November 22, 2005, and accepted for publication February 1, 2006.

Address reprint requests to Dr. Kevin Strange, Vanderbilt University Medical Center, T-4202 Medical Center North, Nashville, TN 37232-2520. Tel.: 615-343-7425; Fax: 615-343-3916; E-mail: kevin.strange@vanderbilt.edu.

© 2006 by the Biophysical Society

0006-3495/06/05/3570/12 \$2.00

doi: 10.1529/biophysj.105.078295

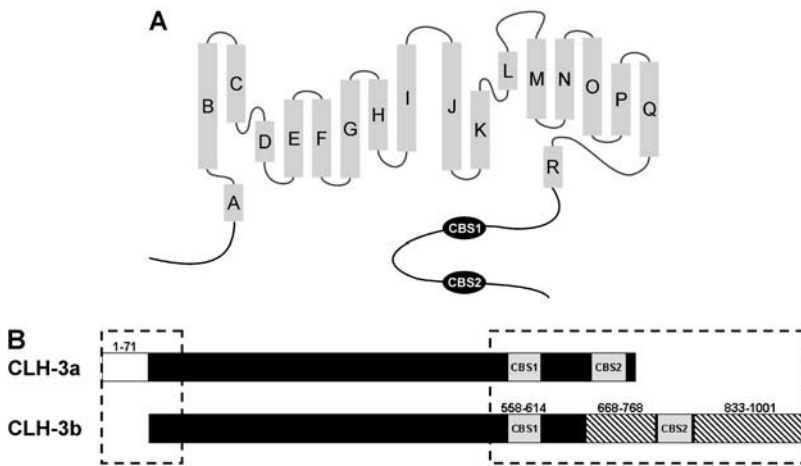


**FIGURE 1** CIC anion channel structural features. (A) Schematic diagram showing basic structural components of eukaryotic CIC anion channels. Shaded rectangles represent  $\alpha$  helices (A–R) identified by x-ray crystallography of a bacterial CIC (5). The cytoplasmic C-terminus of eukaryotic CICs contains two conserved cystathionine- $\beta$ -synthase domains (CBS1 and CBS2). (B) Schematic diagram showing the major differences between the cytoplasmic N- and C-termini (dashed boxes) of CLH-3a and CLH-3b. Major differences between CLH-3a and CLH-3b include a 71 amino acid addition to the N-terminus of CLH-3a (amino acids 1–71), a 101 amino acid insertion between CBS1 and CBS2 in CLH-3b (amino acids 668–768), and a 169 amino acid extension of the CLH-3b C-terminus (amino acids 833–1001).

CLH-3b C-terminal splice insert or deletion of the last 11 amino acids of CBS domain 1 (CBS1) gives rise to functional properties identical to those of CLH-3a. Consistent with studies on other CIC channels (e.g., 4,19,20), voltage-,  $\text{Cl}^-$ , and  $\text{H}^+$ -dependent gating of CLH-3a and CLH-3b are lost when the protopore glutamate gate is mutated to alanine. When the glutamate gate is mutated to cysteine, CLH-3a and CLH-3b exhibit striking differences in the rate of current inhibition by the sulfhydryl reagent MTSET. The differences in MTSET inhibition are reversed by deletion of the same CLH-3b cytoplasmic C-terminal regions that alter channel biophysical properties. Our results indicate that splice variation of the CLH-3b cytoplasmic C-terminus alters extracellular structure and cysteine reactivity and suggest that differences in the conformation of the outer pore vestibule and associated glutamate gate may account for differences in CLH-3a and CLH-3b gating.

## MATERIALS AND METHODS

### Transient expression of CLH-3 constructs

Chimera and truncation mutants were generated by polymerase chain reaction (PCR)-based fusion strategies. Point mutants were generated using a Quikchange kit (Stratagene, La Jolla, CA). All mutants were confirmed by DNA sequencing.

HEK293 (human embryonic kidney) cells were cultured in Eagle's minimal essential medium (MEM; Gibco, Gaithersburg, MD) containing 10% heat-inactivated fetal bovine serum (Gibco), 50 units/ml penicillin, and 50  $\mu\text{g}/\text{ml}$  streptomycin. Cells grown in 35-mm dishes to ~50% confluency were transfected using Superfect reagent (Qiagen, Valencia, CA) with 1  $\mu\text{g}$  green fluorescent protein (GFP) cDNA ligated into pCDNA3 and 5–6  $\mu\text{g}$  wild-type CLH-3a cDNA (kindly provided by Dr. Thomas Jentsch), wild-type CLH-3b cDNA (13), or various CLH-3a and CLH-3b mutant cDNAs ligated into pCDNA3.1. Cells were transfected for 3 h, washed 3 $\times$  with MEM and incubated overnight at 37°C.

### Whole cell patch clamp recording

HEK293 cells were patch clamped ~24 h after transfection. Two hours before initiating electrophysiological experiments, transfected cells were

dissociated by brief exposure to trypsin and then plated onto poly-L-lysine-coated coverslips. Plated coverslips were placed in a bath chamber mounted onto the stage of an inverted microscope. Cells were visualized by fluorescence and differential interference contrast (DIC) microscopy.

Transfected cells were identified by GFP fluorescence and patch clamped using a bath solution containing 90 mM *n*-methyl-D-glucamine (NMDG)-Cl, 5 mM  $\text{MgSO}_4$ , 1 mM  $\text{CaCl}_2$ , 12 mM Hepes, 8 mM Tris, 5 mM glucose, 80 mM sucrose, and 2 mM glutamine (pH 7.4, 300 mOsm), and a pipette solution containing 116 mM NMDG-Cl, 2 mM  $\text{MgSO}_4$ , 20 mM Hepes, 6 mM CsOH, 1 mM EGTA, 2 mM ATP, 0.5 mM GTP, and 10 mM sucrose (pH 7.2, 275 mOsm). In low bath  $\text{Cl}^-$  experiments, NMDG-Cl was partially replaced with NMDG-gluconate.

Patch electrodes were pulled from 1.5-mm outer diameter silanized borosilicate microhematocrit tubes; electrode resistance ranged from 2–4 M $\Omega$ . Currents were measured with an Axopatch 200B (Axon Instruments, Foster City, CA) patch clamp amplifier. Electrical connections to the patch clamp amplifier were made using Ag/AgCl wires and 3 M KCl/agar bridges. Data acquisition and analysis were performed using pClamp 8 software (Axon Instruments).

Cells were voltage clamped at a holding potential of 0 mV, and currents were elicited by stepping membrane voltage to values from –120 mV to +80 mV in 20 mV steps. Current-to-voltage (*I*-*V*) relationships were constructed from mean current values recorded over the last 20 ms of voltage steps. CLH-3 channel voltage sensitivity is not accurately described by half-activation potentials derived from Boltzmann analyses (14). We therefore estimated channel activation voltage from *I*-*V* relationships as described previously (14). Briefly, wild-type and mutant CLH-3 channels activated between –20 mV and –40 mV or –60 mV and –100 mV. Activation voltage was determined by fitting a straight line between –40 mV and –60 mV or –80 mV and –100 mV on *I*-*V* curves and extrapolating back to the zero current voltage. The zero current intercept of this line is defined as the activation voltage.

### MTSET inhibition experiments

[2-(Trimethylammonium)ethyl] methanethiosulfonate bromide (MTSET; Toronto Research Chemicals, Toronto, Ontario, Canada) was dissolved in water as a 400 mM stock and stored in 100  $\mu\text{l}$  aliquots at –80°C until use. Single aliquots were added to 40 ml of control bath immediately before each experiment. The final MTSET working concentration was 1 mM.

Whole cell current amplitude in MTSET experiments was recorded by stepping membrane voltage to –100 mV for 500 ms every 1 s from a holding potential 0 mV. The bath was perfused continuously with control solution during this voltage clamp protocol. Cells were exposed to MTSET-containing bath solution after whole cell current reached stable levels.

Continuous bath perfusion was maintained until MTSET inhibition was complete.

## Statistical analyses

Data are presented as means  $\pm$  SE. Statistical significance was determined using Student's two-tailed *t*-test or ANOVA. *p* values of  $\leq 0.05$  were taken to indicate statistical significance.

## RESULTS

### Splice variation of the C-terminus regulates CLH-3b voltage, $\text{Cl}^-$ , and $\text{H}^+$ sensitivity

Fig. 1 A is a schematic diagram showing the basic structural features of eukaryotic CIC channels. The channels are composed of 18  $\alpha$ -helical domains and intracellular N- and C-termini. Two CBS domains joined by a linker region of variable length are present in the cytoplasmic C-terminus (5,11).

A block diagram showing the major primary structure differences between CLH-3a and CLH-3b is shown in Fig. 1 B (see Denton et al. (14) for alignment of the CLH-3a and

CLH-3b amino acid sequences). The major differences between the channels include a 71 amino acid N-terminal extension on CLH-3a (amino acids 1–71), a 101 amino acid insertion between CBS1 and CBS2 on CLH-3b (amino acids 668–768), and 169 amino acid extension of the CLH-3b C-terminus (amino acids 833–1001) (14).

Figs. 2 and 3 show the major functional differences between wild-type CLH-3a and CLH-3b. The two channels exhibit striking differences in voltage sensitivity. Transfected cells were held at 0 mV and then voltage clamped for 3 s at conditioning voltages of  $-20$  to  $+60$  mV before stepping to  $-120$  mV for 2 s to activate the channels. CLH-3a activity was potentiated by prepolarization whereas it had no effect on CLH-3b activity (Fig. 2, A and B). Conditioning depolarization also induced slow inactivation of CLH-3a but had no effect on CLH-3b (Fig. 2 C).

CLH-3a and CLH-3b exhibited different sensitivities to hyperpolarizing voltages and extracellular ions. Mean activation voltages for CLH-3a and CLH-3b were  $-68$  mV and  $-32$  mV, respectively (Figs. 3, A and B). Lowering extra-

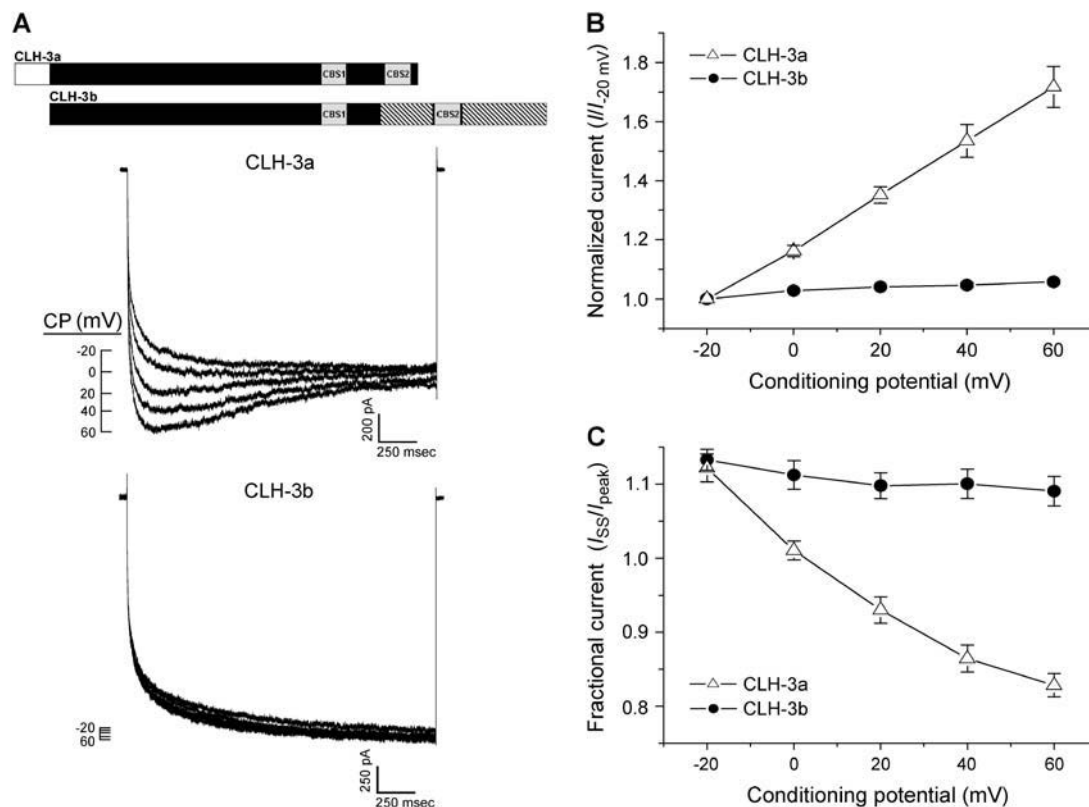
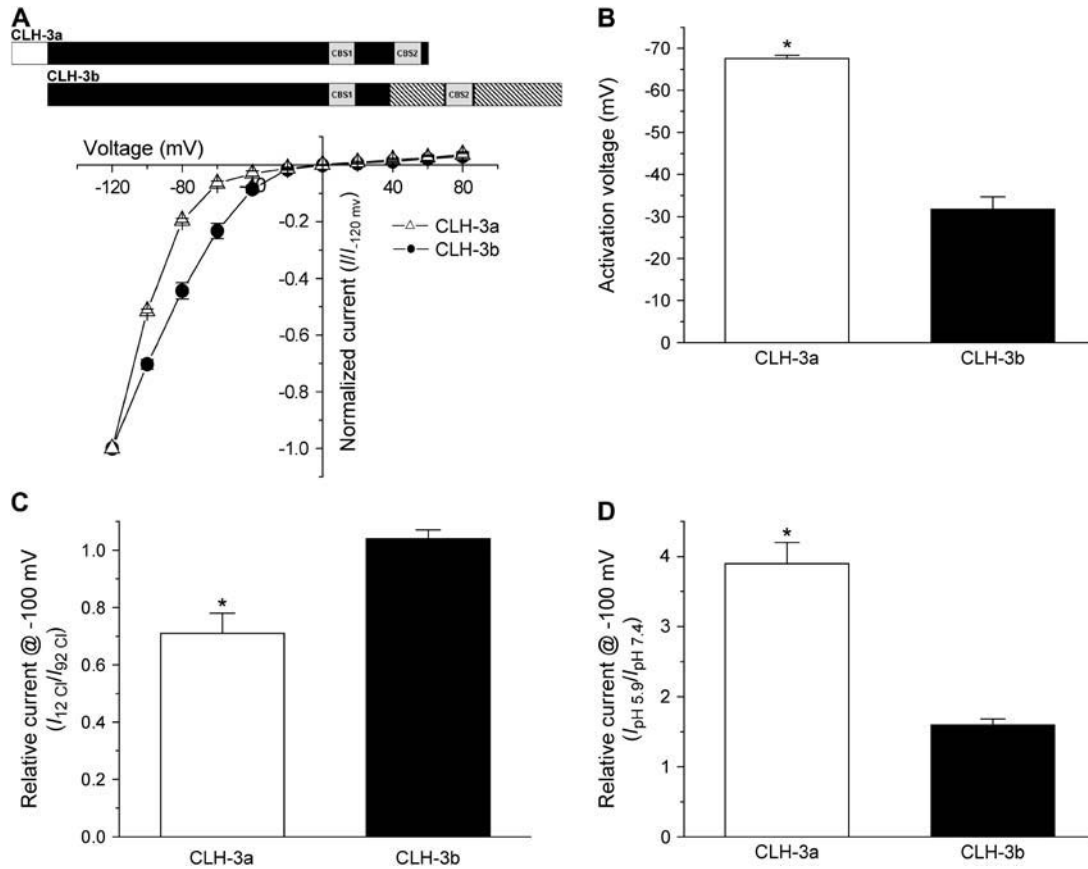


FIGURE 2 Effect of depolarizing conditioning potentials (CP) on wild-type CLH-3a and CLH-3b. (A) Representative current traces from HEK293 cells cotransfected with GFP and mutant channel cDNAs. Cells were held at conditioning voltages of  $-20$  mV to  $+60$  mV for 3 s and then voltage clamped at  $-120$  mV to activate heterologously expressed channels. A schematic diagram of the wild-type CLH-3a and CLH-3b channels is shown above the current traces. (B) Effect of conditioning potential (CP) on hyperpolarization-induced current activation. Peak current amplitude was measured between 170 ms and 270 ms after stepping to  $-120$  mV. Current values were normalized to that measured following a conditioning pulse of  $-20$  mV (i.e.,  $I_{-20\text{ mV}}$ ). Values are means  $\pm$  SE ( $n = 6-7$ ). (C) Effect of CP on current inactivation. Mean normalized pseudo-steady-state current ( $I_{SS}$ ) was measured over the last 20 ms of the  $-120$  mV test pulse and normalized to peak current ( $I_{\text{peak}}$ ) amplitude. Values are means  $\pm$  SE ( $n = 6-7$ ). Predepolarization induces current potentiation and inactivation only in CLH-3a.



**FIGURE 3** Voltage,  $\text{Cl}^-$ , and  $\text{H}^+$  sensitivity of wild-type CLH-3a and CLH-3b. (A, B) *I-V* relationships and activation voltages. Whole cell  $\text{Cl}^-$  currents were evoked by stepping membrane voltage for 1 s between  $-120$  mV and  $+80$  mV in  $20$ -mV increments from a holding potential of  $0$  mV. Each test pulse was followed by a  $4$ -s interval at  $0$  mV. *I-V* plots are normalized to the steady-state current measured at  $-120$  mV. Values are means  $\pm$  SE ( $n = 6-7$ ). \* $p < 0.0001$  compared to CLH-3b. A schematic diagram of the wild-type CLH-3a and CLH-3b channels is shown above the *I-V* plots. (C) Effect of reducing bath  $\text{Cl}^-$  concentration from  $92$  mM to  $12$  mM on whole cell current amplitude measured at  $-100$  mV. Current amplitude was normalized to that measured at  $92$  mM  $\text{Cl}^-$  ( $I_{92\text{ Cl}^-}$ ). Values are means  $\pm$  SE ( $n = 8-9$ ). \* $p < 0.0004$  compared to CLH-3b. Relative current for CLH-3b is not significantly different from  $1$  ( $p > 0.2$ ). (D) Effect of bath pH on whole cell current amplitude measured at  $-100$  mV. Current amplitude was normalized to that measured at pH  $7.4$  ( $I_{\text{pH } 7.4}$ ). Values are means  $\pm$  SE ( $n = 8-9$ ). \* $p < 0.0001$  compared to CLH-3b. CLH-3a requires stronger hyperpolarization for activation compared to CLH-3b. In addition, CLH-3a is more sensitive to extracellular  $\text{H}^+$  and is inhibited by reducing bath  $\text{Cl}^-$  concentration.

cellular  $\text{Cl}^-$  concentration from  $92$  mM to  $12$  mM inhibited CLH-3a activity  $\sim 29\%$  but had no inhibitory effect on CLH-3b (Fig. 3 C). Decreasing extracellular pH from  $7.4$  to  $5.9$  increased CLH-3a and CLH-3b activity  $3.9$ -fold and  $1.6$ -fold, respectively (Fig. 3 D).

The differences in the functional properties of the two channels could be due either to splice insert of the unique  $71$  amino acid N-terminus onto CLH-3a and/or addition of the two splice inserts into the C-terminus of CLH-3b (see Fig. 1 B). To determine whether the  $71$  amino acid N-terminus of CLH-3a modulates channel gating, we created a CLH-3a N-terminal deletion mutant, CLH-3a $\Delta 1-71$ , and a chimera of CLH-3a and CLH-3b, CLH-3a/b, in which the first  $71$  amino acids of CLH-3a were fused to the CLH-3b N-terminus.

As shown in Figs. 4 and 5, neither deletion of the  $71$  amino acid N-terminus of CLH-3a nor addition of this domain to CLH-3b had any effect on channel properties. CLH-3a $\Delta 1-71$  and CLH-3a/b exhibited the same basic functional charac-

teristics as wild-type CLH-3a and CLH-3b, respectively. Like wild-type CLH-3a, CLH-3a $\Delta 1-71$  was sensitive to depolarizing conditioning voltages (Fig. 4, A and B), required strong hyperpolarization ( $\sim -70$  mV) for activation (Fig. 5, A and B), was inhibited by reduction of bath  $\text{Cl}^-$  concentration (Fig. 5 C), and was activated more than fourfold by reduction of bath pH from  $7.4$  to  $5.9$  (Fig. 5 D). In contrast, the CLH-3a/b chimera retained CLH-3b-like properties. CLH-3a/b was insensitive to depolarizing conditioning voltages (Fig. 4, A and B) and reduction of bath  $\text{Cl}^-$  (Fig. 5 C), had an activation voltage of  $\sim -28$  mV (Fig. 5 A and B), and was activated less than twofold by a pH  $5.9$  bath solution (Fig. 5 D). Taken together, these results demonstrate that the  $71$  amino acid N-terminal splice insert on CLH-3a does not modulate channel voltage, pH, or  $\text{Cl}^-$  sensitivity.

To test the role of splice variation of the C-terminus in regulating channel gating, we deleted separately the two CLH-3b splice inserts (see Fig. 1 B). Deletion of the most

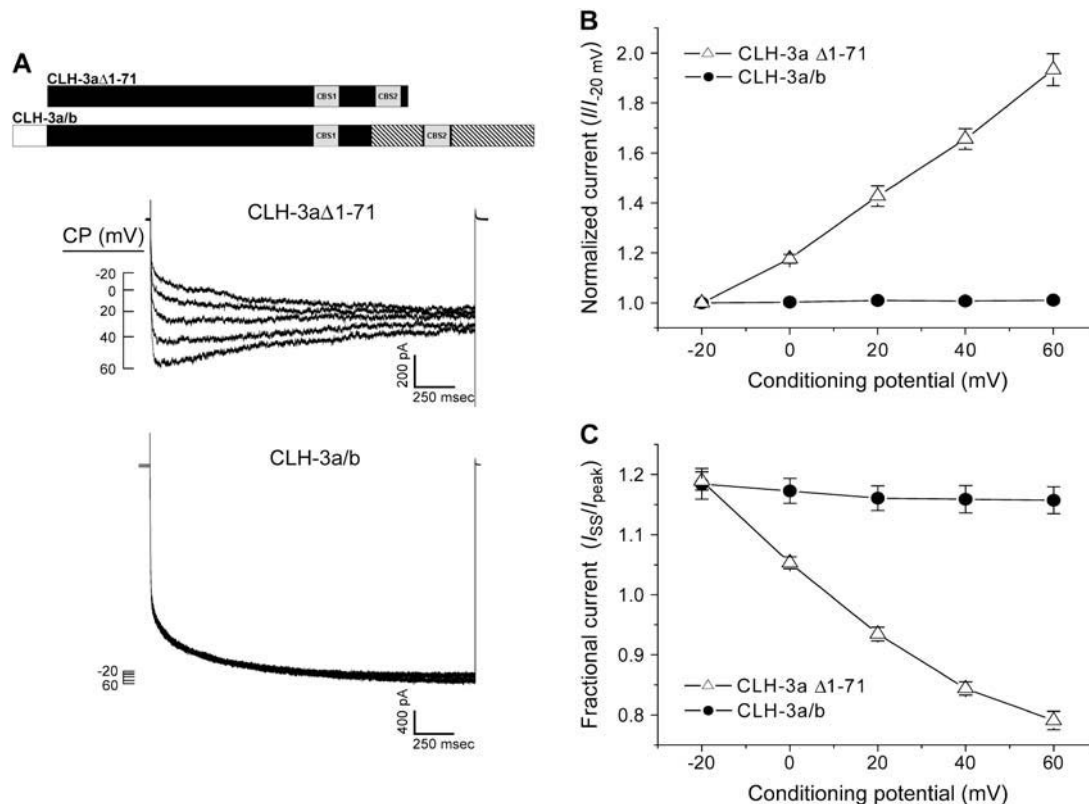


**FIGURE 4** Effect of depolarizing CPs on CLH-3aΔ1-71 and CLH-3a/b. (A) Representative current traces from HEK293 cells cotransfected with GFP and mutant channel cDNAs. Voltage clamp protocol was the same as that shown in Fig. 2 A and described in Fig. 2 legend. A schematic diagram of the CLH-3aΔ1-71 and CLH-3a/b mutant channels is shown above the current traces. (B) Effect of CP on hyperpolarization-induced current activation. Peak current amplitude was measured between 170 ms and 270 ms after stepping to  $-120$  mV. Current values were normalized to that measured following a conditioning pulse of  $-20$  mV (i.e.,  $I_{-20\text{ mV}}$ ). Values are means  $\pm$  SE ( $n = 8-10$ ). (C) Effect of CP on current inactivation. Mean normalized pseudo-steady-state current ( $I_{SS}$ ) was measured over the last 20 ms of the  $-120$  mV test pulse and normalized to peak current ( $I_{peak}$ ) amplitude. Values are means  $\pm$  SE ( $n = 8-10$ ). Predepolarization induces current potentiation and inactivation only in CLH-3aΔ1-71.

C-terminal splice insert (amino acids 833–1001) gave rise to CLH-3a-like functional properties. CLH-3b( $\Delta 833-1001$ ) was potentiated by depolarizing conditioning voltages (Fig. 6) and exhibited reduced sensitivity to hyperpolarizing voltages and increased sensitivity to extracellular  $\text{Cl}^-$  and  $\text{H}^+$  (Fig. 7). The voltage,  $\text{Cl}^-$ , and  $\text{H}^+$  sensitivity of CLH-3b( $\Delta 833-1001$ ) fully recapitulates that of wild-type CLH-3a (Figs. 2 and 3).

Deletion of the 101 amino acid splice insert located between CBS1 and CBS2 of CLH-3b (amino acids 668–768) did not alter channel sensitivity to depolarizing conditioning voltages (Fig. 6) or sensitivity to  $\text{Cl}^-$  and  $\text{H}^+$  (Fig. 7, D and E). However, CLH-3b( $\Delta 668-768$ ) exhibited significantly ( $p < 0.0001$  compared to wild-type CLH-3b; see Fig. 3 B) reduced sensitivity to hyperpolarizing voltages (Fig. 7 B).

CLH-3b( $\Delta 668-768$ ) also had altered kinetics of hyperpolarization-induced current activation (Fig. 7 C). As we have described previously (17), voltage-dependent activation of wild-type CLH-3b is well described by the sum of two exponentials that define fast and slow time constants ( $\tau_{fast}$  and  $\tau_{slow}$ ). The inset in Fig. 7 C shows a single exponential fit to a

wild-type CLH-3b current activated by a test voltage of  $-120$  mV. The fit is poor as evidenced by a mean  $\pm$  SE coefficient of determination ( $R^2$ ) of  $0.85 \pm 0.02$  ( $n = 7$ ). Mean  $\pm$  SE  $\tau_{fast}$  and  $\tau_{slow}$  derived from double exponential fits were  $5.3 \pm 0.7$  ms and  $135 \pm 10$  ms ( $n = 7$ ), respectively.

In contrast to wild-type CLH-3b, activation of CLH-3b( $\Delta 668-768$ ) at  $-120$  mV was well described by a single exponential function (Fig. 7 C). The mean  $\pm$  SE  $R^2$  value for the fit was  $0.99 \pm 0.001$  ( $n = 13$ ). The mean  $\pm$  SE time constant of CLH-3b( $\Delta 668-768$ ) activation derived from the single exponential fit was  $83 \pm 4$  ms ( $n = 13$ ). As described in more detail in the Discussion section, the activation voltage and kinetics of hyperpolarization-induced activation of CLH-3b( $\Delta 668-768$ ) resemble those of wild-type CLH-3b coexpressed heterologously with and inhibited by the Ste20 kinase GCK-3 (17).

The *C. elegans* Gene Knockout Project at the Oklahoma Medical Research Foundation recently generated a *clh-3* deletion mutant worm strain. Genomic sequencing and PCR analysis demonstrated that the *clh-3(ok768)* allele deletes amino acids 668–768 (i.e., the 101 amino acid splice insert

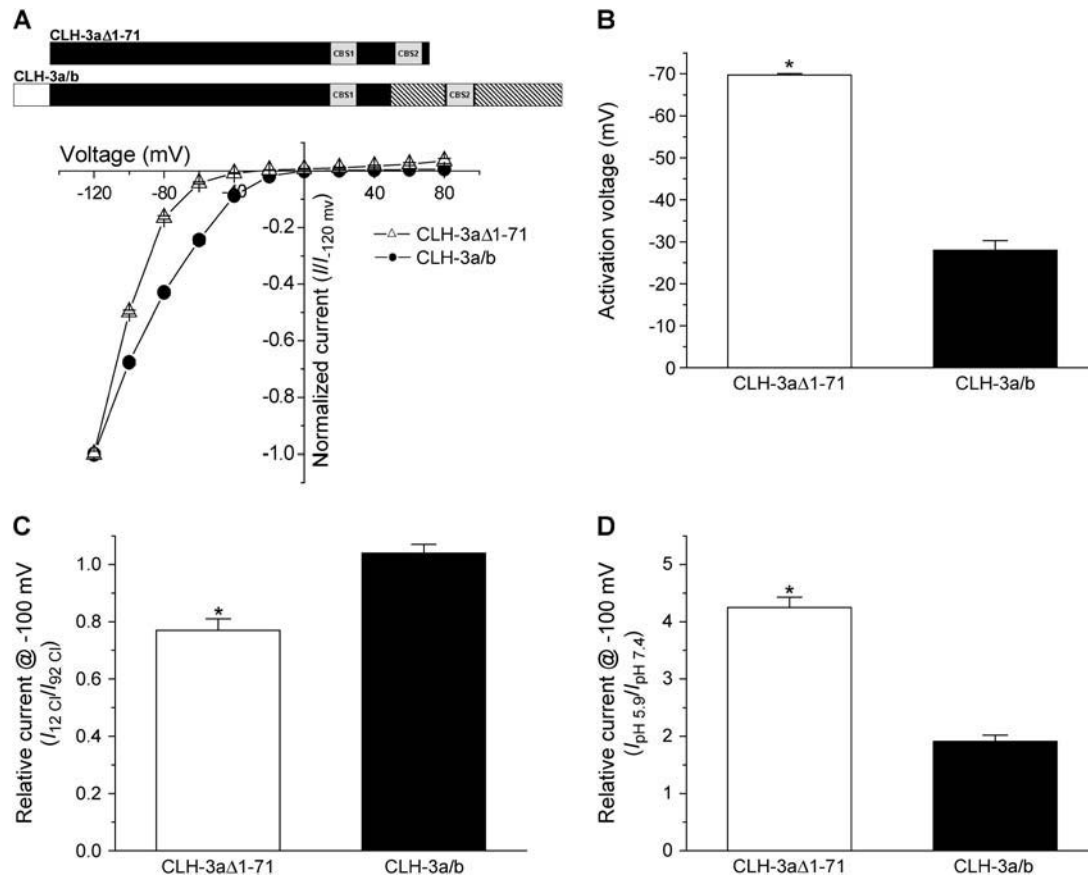


FIGURE 5 Voltage,  $\text{Cl}^-$ , and  $\text{H}^+$  sensitivity of CLH-3a $\Delta$ 1-71 and CLH-3a/b. (A, B)  $I$ - $V$  relationships and activation voltages. Voltage clamp protocol is the same as that described in the Fig. 3 A legend.  $I$ - $V$  plots are normalized to the steady-state current measured at  $-120$  mV. Values are means  $\pm$  SE ( $n = 8$ – $9$ ).  $*p < 0.0001$  compared to CLH-3a/b. A schematic diagram of the CLH-3a $\Delta$ 1-71 and CLH-3a/b mutant channels is shown above the  $I$ - $V$  plots. (C) Effect of reducing bath  $\text{Cl}^-$  concentration from 92 mM to 12 mM on whole cell current amplitude measured at  $-100$  mV. Current amplitude was normalized to that measured at 92 mM  $\text{Cl}^-$  ( $I_{92 \text{ Cl}}$ ). Values are means  $\pm$  SE ( $n = 4$ – $5$ ).  $*p < 0.0001$  compared to CLH-3a/b. Relative current for CLH-3a/b is not significantly different from 1 ( $p > 0.3$ ). (D) Effect of bath pH on whole cell current amplitude measured at  $-100$  mV. Current amplitude was normalized to that measured at pH 7.4 ( $I_{\text{pH } 7.4}$ ). Values are means  $\pm$  SE ( $n = 8$ – $9$ ).  $*p < 0.0001$  compared to CLH-3a/b. CLH-3a $\Delta$ 1-71 requires stronger hyperpolarization for activation compared to CLH-3a/b. In addition, CLH-3a $\Delta$ 1-71 is more sensitive to extracellular  $\text{H}^+$  and is inhibited by reducing bath  $\text{Cl}^-$  concentration.

between CBS1 and CBS2) of CLH-3b as well as an additional 64 amino acids immediately upstream (i.e., amino acids 604–667; 21; see Fig. 1 B). The mutant channel, CLH-3b( $\Delta$ 604–768), is expressed functionally in the worm oocyte and exhibits CLH-3a-like voltage,  $\text{Cl}^-$ , and  $\text{H}^+$  sensitivity (21). These observations indicate that amino acids 604–667 also control CLH-3b functional properties.

As noted earlier, all eukaryotic CIC channels possess two C-terminal CBS domains. Mutations in these domains alter voltage-dependent gating of various CIC channels (22,23). Paired CBS domains are also found in numerous unrelated proteins, and mutations in them give rise to diverse human diseases (11). Given the importance of CBS domains in protein function, we postulated that the altered gating properties of the CLH-3b( $\Delta$ 604–768) mutant (21) are due at least in part to deletion of the last 11 amino acids of CBS1 (i.e., amino acids 604–614).

To test this hypothesis, we generated two mutant channels by deleting amino acids 604–614 of CBS1 or amino acids

615–667, which are immediately downstream of the predicted CBS1 domain. CLH-3b( $\Delta$ 615–667) had CLH-3b-like functional properties. The channel was insensitive to depolarizing conditioning voltages and had extracellular  $\text{Cl}^-$  and pH sensitivities that were CLH-3b-like (data not shown). However, CLH-3b( $\Delta$ 615–667) did exhibit a significant ( $p < 0.0001$  compared to wild-type CLH-3b) shift in activation voltage to a mean value of  $-64$  mV.

In contrast to CLH-3b( $\Delta$ 615–667), the CBS1 domain mutant, CLH-3b( $\Delta$ 604–614), had functional properties that were indistinguishable from wild-type CLH-3a (Figs. 2 and 3). Conditioning prepolarization-potentiated hyperpolarization induced activation of CLH-3b( $\Delta$ 604–614) and caused slow channel inactivation (Fig. 6). CLH-3b( $\Delta$ 604–614) also exhibited a hyperpolarizing shift in activation voltage (Fig. 7 B) and increased sensitivity to extracellular  $\text{H}^+$  (Fig. 7 D) and bath  $\text{Cl}^-$  reduction (Fig. 7 E).

In summary, data in Figs. 2–7 demonstrate clearly that the 71 amino acid N-terminal splice insert on CLH-3a does not

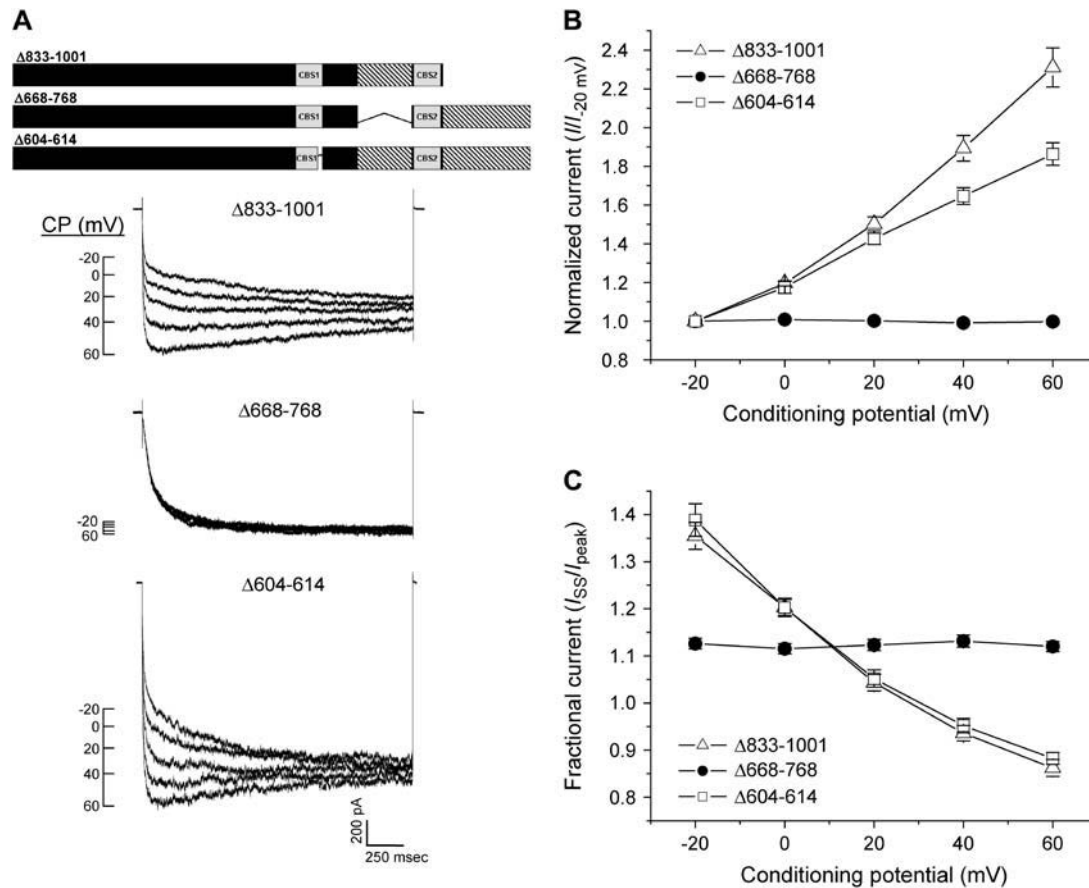


FIGURE 6 Effect of C-terminal deletion mutations on CLH-3b sensitivity to depolarizing CPs. (A) Representative current traces from HEK293 cells cotransfected with GFP and mutant CLH-3b cDNAs. Voltage clamp protocol was the same as that described in Fig. 2 legend. A schematic diagram of the CLH-3b(Δ833-1001), CLH-3b(Δ668-768), and CLH-3b(Δ604-614) mutant channels is shown above the current traces. (B, C) Effect of CP on hyperpolarization-induced current activation and inactivation. Current amplitudes were measured and normalized as described in Fig. 2 legend. Values are means  $\pm$  SE ( $n = 5-14$ ). Deletion of the last 169 amino acids of CLH-3b or deletion of the last 11 amino acids of CBS1 sensitizes the channel to depolarizing conditioning voltages.

modulate channel voltage,  $\text{Cl}^-$ , or pH sensitivity. Instead, C-terminal splice variation alters channel functional properties and gives rise to the unique biophysical characteristics of CLH-3b. The results also suggest that a functional interaction exists between the last 169 amino acid splice insert of CLH-3b and the C-terminal portion of CBS1.

### Splice variation of the cytoplasmic C-terminus alters reactivity of extracellular cysteine residues to MTSET

The bacterial CIC crystal structure revealed the presence of three  $\text{Cl}^-$  binding sites in the ion permeation pathway (4). These binding sites are formed by isoleucine and phenylalanine, serine, and tyrosine residues located on the N-terminal ends of helices N, D, and R, respectively (see Fig. 1). In the closed channel conformation, the carboxyl group of a glutamate residue located on the N-terminus of helix F occupies the  $\text{Cl}^-$  binding site closest to the extracellular solution. This glutamate residue is highly conserved throughout the CIC

superfamily and appears to mediate the so-called fast gating mechanism that controls the opening of each protopore (4,19,20,24). Chloride and  $\text{H}^+$  are thought to activate CIC channels by displacing or protonating this so-called glutamate gate.

Dutzler et al. (5) suggested that the linkage of the CIC selectivity filter and glutamate gate in the outer pore vestibule to the cytoplasmic C-terminus via the R helix could provide a direct route for regulating channel activity by intracellular signaling events. Alignment of CLH-3a and CLH-3b with the *Salmonella* CIC sequence revealed that the glutamate gate is conserved in both splice variants. In addition, isoleucine, phenylalanine, serine, and tyrosine residues that form  $\text{Cl}^-$  binding sites are also conserved. Based on the conservation of this primary structure, we proposed that splice variation of the cytoplasmic C-terminus may secondarily alter via the R helix the conformation of the selectivity filter and glutamate gate, which in turn gives rise to the differences in CLH-3a and CLH-3b voltage,  $\text{Cl}^-$ , and  $\text{H}^+$  sensitivity (14). To begin testing this hypothesis, we mutated

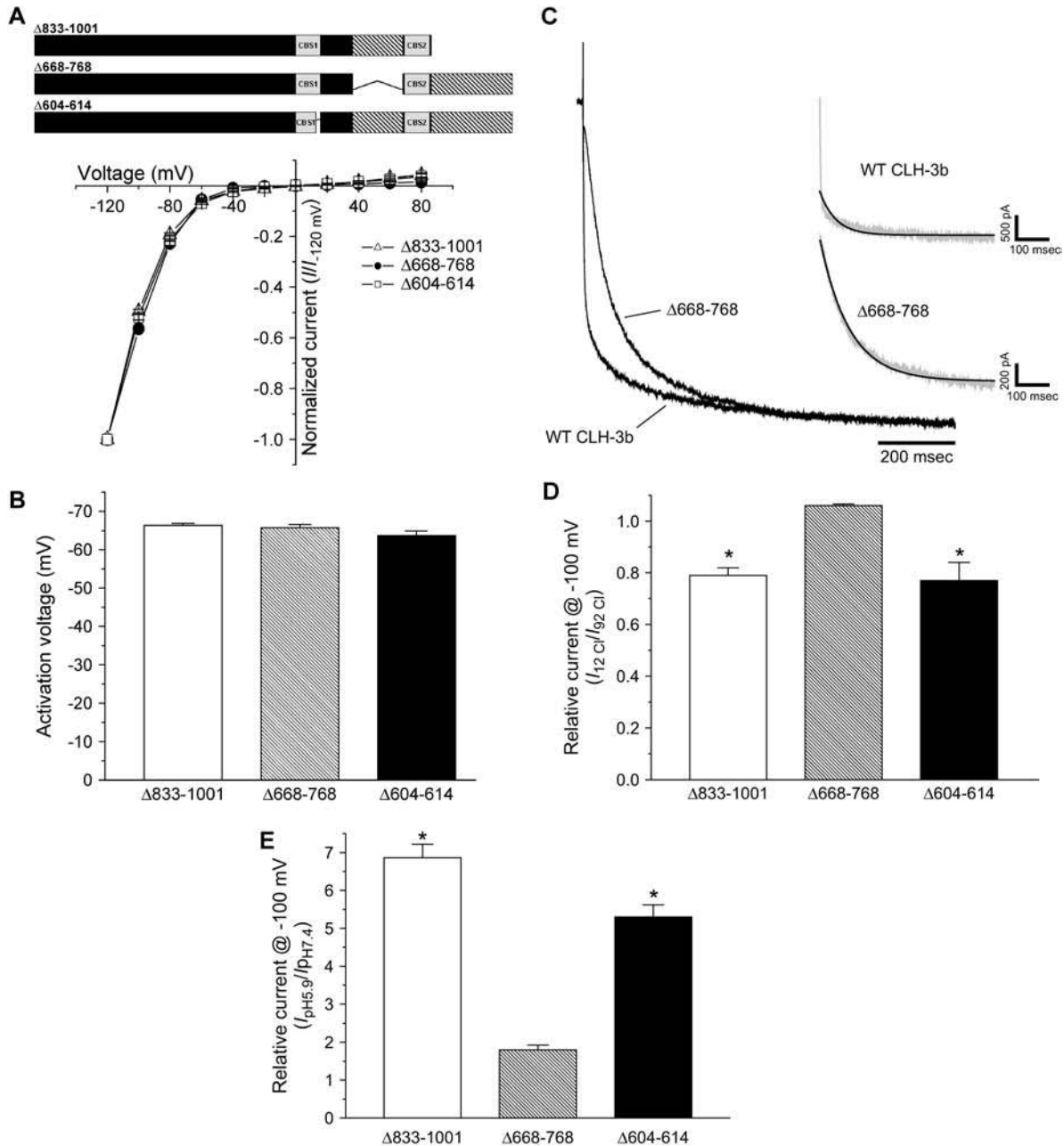


**FIGURE 7** Voltage,  $\text{Cl}^-$ , and  $\text{H}^+$  sensitivity of CLH-3b C-terminal deletion mutants. (A, B)  $I$ - $V$  relationships and activation voltages. Whole cell  $\text{Cl}^-$  currents were evoked and activation voltages determined as described in Fig. 3 legend. Values are means  $\pm$  SE ( $n = 8$ –13). A schematic diagram of the CLH-3b( $\Delta 833$ -1001), CLH-3b( $\Delta 668$ -768), and CLH-3b( $\Delta 604$ -614) mutant channels is shown above the  $I$ - $V$  plot. (C) Mean relative current traces of cells expressing wild-type CLH-3b or  $\Delta 668$ -768 ( $n = 7$ –13). Gray inset traces are examples of wild-type CLH-3b and  $\Delta 668$ -768 currents. Black overlay traces are single exponential fits to the first 500 ms of current activation (17). (D) Effect of reducing bath  $\text{Cl}^-$  concentration from 92 mM to 12 mM on whole cell current amplitude measured at  $-100$  mV. Current amplitude was normalized to that measured at 92 mM  $\text{Cl}^-$  ( $I_{92\text{ Cl}^-}$ ). Values are means  $\pm$  SE ( $n = 6$ –11).  $*p < 0.01$  compared to  $\Delta 668$ -768. (E) Effect of bath pH on whole cell current amplitude measured at  $-100$  mV. Current amplitude was normalized to that measured at pH 7.4 ( $I_{\text{pH}7.4}$ ). Values are means  $\pm$  SE ( $n = 5$ –12).  $*p < 0.001$  compared to  $\Delta 668$ -768. Deletion of the last 169 amino acids of CLH-3b or deletion of the last 11 amino acids of CBS1 reduces the channel sensitivity to hyperpolarizing voltages and increases sensitivity to extracellular  $\text{Cl}^-$  and  $\text{H}^+$ .

E-238 and E-167 in CLH-3a and CLH-3b, respectively, to alanine. Data in Fig. 8 demonstrate that the glutamate mutants are constitutively active (Figs. 8, A–C) and are largely insensitive to extracellular acidification (Fig. 8 F). In addition, CLH-3a(E238A) is not potentiated by conditioning

depolarization (Fig. 8 D) nor is it inhibited by lowering extracellular  $\text{Cl}^-$  from 92 mM to 12 mM (Fig. 8 E).

To begin assessing whether CLH-3a and CLH-3b exhibit differences in outer pore conformation, we mutated E-238 and E-167 to cysteine and characterized the effect of the

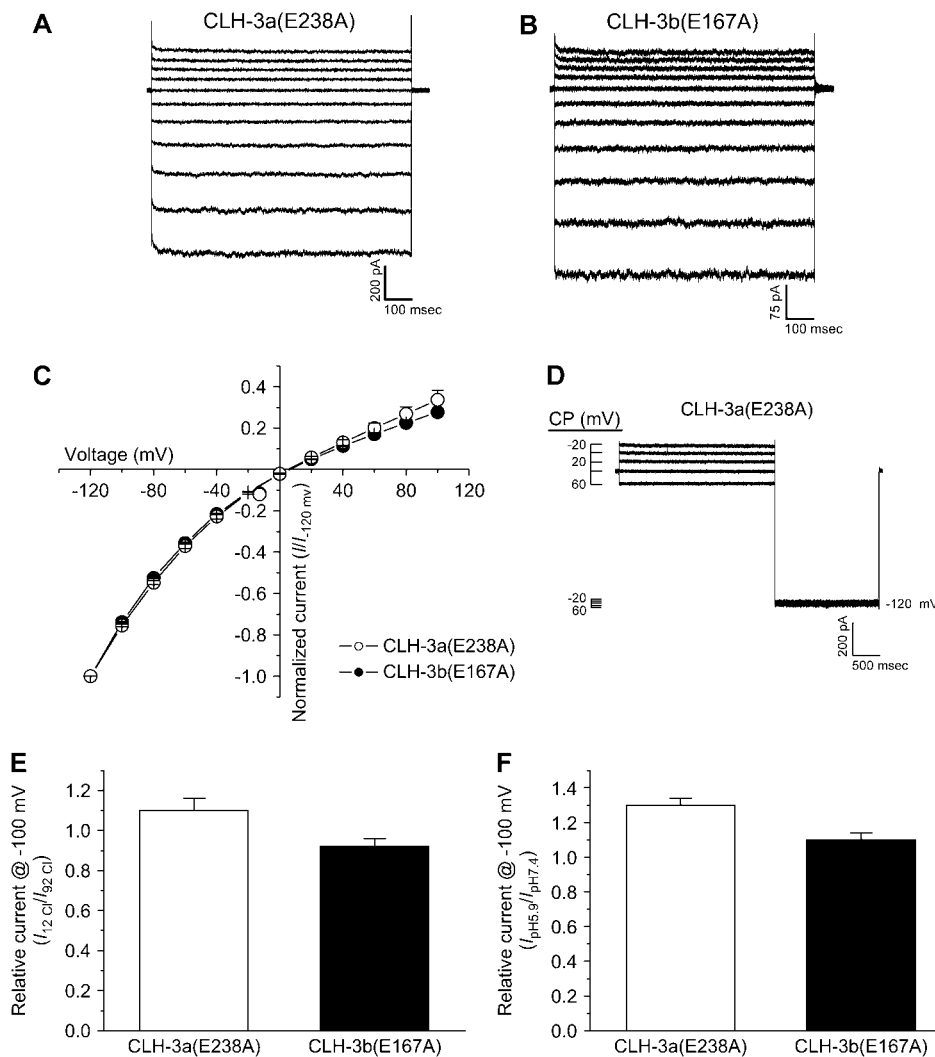


**FIGURE 8** Voltage,  $\text{Cl}^-$ , and  $\text{H}^+$  sensitivity of CLH-3a and CLH-3b glutamate gate mutants. (A, B) Representative current traces from HEK293 cells cotransfected with GFP and CLH-3a(E238A) or CLH-3b(E167A) mutant cDNAs. Whole cell  $\text{Cl}^-$  currents were evoked by stepping membrane voltage for 1 s between  $-120$  mV and  $+80$  mV in  $20$ -mV increments from a holding potential of  $0$  mV. Each test pulse was followed by a  $4$ -s interval at  $0$  mV. Time-dependent hyperpolarization-induced activation is lost in both channels. (C)  $I$ - $V$  relationships for CLH-3a(E238A) or CLH-3b(E167A). Values are means  $\pm$  SE ( $n = 7$ ). (D) Effect of depolarizing conditioning voltages on CLH-3a(E238A). Voltage clamp protocol is the same as that described in Fig. 2 legend. Whole cell currents are shown at both the conditioning voltages and  $-120$  mV. (E, F) Effect of low bath  $\text{Cl}^-$  (E) and bath acidification (F) on whole cell current measured at  $-100$  mV. Values are means  $\pm$  SE ( $n = 5$ - $6$ ). Mutating the glutamate gate to alanine constitutively activates CLH-3a and CLH-3b and dramatically reduces activation by bath acidification in both channels. CLH-3a(E238A) is also insensitive to bath  $\text{Cl}^-$  and conditioning depolarizing voltages.

positively charged cysteine modifying reagent MTSET on channel activity. Fig. 9 A shows the inhibitory effect of  $1$  mM MTSET on wild-type CLH-3a and CLH-3b and on the CLH-3a(E238C), CLH-3b(E167C), CLH-3b(E167C) $\Delta$ 833-1001, and CLH-3b(E167C) $\Delta$ 604-614 mutant channels. MTSET inhibited wild-type CLH-3a and CLH-3b by  $40$ - $50\%$ . Mutation of the glutamate gate to cysteine significantly ( $p < 0.01$ ) increased the extent of current inhibition induced by MTSET in all four mutant channels. Mean percent inhibition of the four cysteine mutants examined were  $65$ - $75\%$ . The increased inhibitory effect of MTSET on the glutamate gate cysteine mutants indicates that the engineered cysteine residue contributes to MTSET inhibition and/or that the mutation has altered reactivity of endogenous extracellular cysteine residues.

Fig. 9 B shows examples of the time courses of MTSET inhibition on currents in cells expressing CLH-3a(E238C), CLH-3b(E167C), or CLH-3b(E167C) $\Delta$ 833-1001. MTSET inhibits the three currents in a monoexponential fashion. The time constants of MTSET inhibition derived from exponential fits to current records such as those in Fig. 9 B are shown

in Fig. 9 C. Mean inhibition time constants for wild-type CLH-3a and CLH-3b were  $24$  s and  $18$  s, respectively, and were not significantly ( $p > 0.2$ ) different. Mutating E-238 to cysteine in CLH-3a had no significant ( $p > 0.9$ ) effect on the inhibition time constant (mean time constant =  $24$  s). However, MTSET inhibition of CLH-3b(E167C) was dramatically slowed. The mean inhibition time constant was increased significantly ( $p < 0.001$ ) from  $18$  s for wild-type CLH-3b to  $144$  s for the CLH-3b(E167C) mutant (Fig. 9 C). These results demonstrate that the engineered cysteine residue and/or endogenous extracellular cysteines in CLH-3b(E167C) have altered MTSET reactivity compared to cysteine residues in CLH-3a(E238C).

To test the hypothesis that the structure of the C-terminus secondarily alters structural relationships on the outer surface of the channel, we quantified the effect of C-terminal deletion mutations on MTSET inhibition of CLH-3b(E167C). Deletion mutations in CLH-3b that gave rise to CLH-3a-like functional properties (see Figs. 6 and 7) had no effect on the extent of MTSET inhibition (Fig. 9 A) but dramatically reduced the MTSET inhibition time constant. Mean inhibition

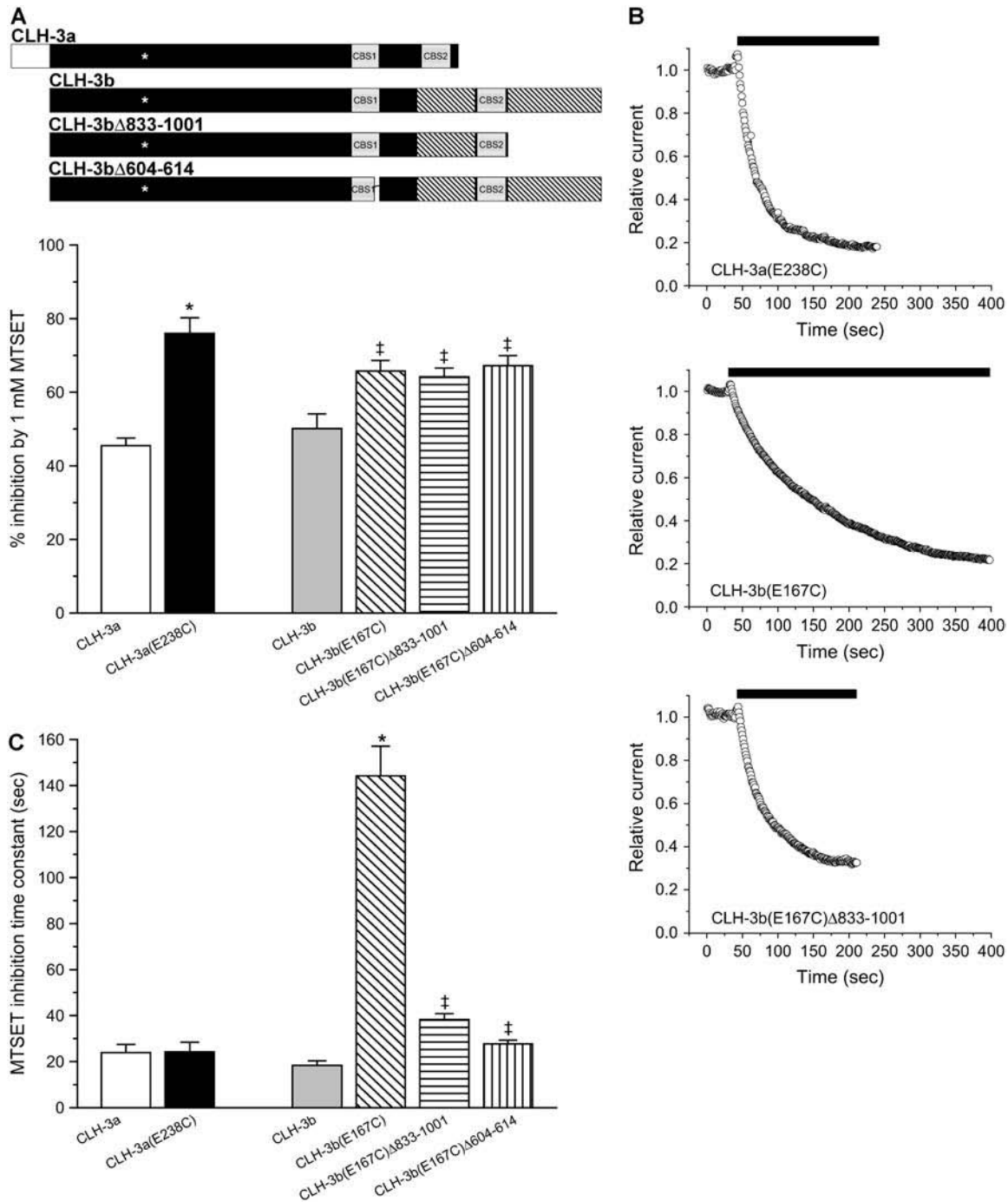


FIGURE 9 Effect of MTSET on wild-type CLH-3a and CLH-3b and glutamate gate cysteine mutants. (A) Percent inhibition of 1 mM MTSET on cells expressing wild-type or mutant channels. Values are means  $\pm$  SE ( $n = 6-13$ ).  $*p < 0.0001$  compared to wild-type CLH-3a.  $^{\ddagger}p < 0.01$  compared to wild-type CLH-3b. A schematic diagram of the wild-type CLH-3a, wild-type CLH-3b, CLH-3b( $\Delta$ 833-1001), and CLH-3b( $\Delta$ 604-614) channels is shown above the plot. Asterisks indicate approximate location of glutamate-to-cysteine mutation. (B) Representative plots showing the effect of 1 mM MTSET (black bars) on whole cell currents in cells expressing CLH-3a(E238C), CLH-3b(E167C), or CLH-3b(E167C) $\Delta$ 833-1001. Cells were voltage clamped at  $-100$  mV, and whole cell currents were recorded at 1 s intervals before and during exposure to MTSET (black bar). (C) MTSET inhibition time constants. Time constants were determined by fitting a single exponential function to plots such as those shown in panel B. Values are means  $\pm$  SE ( $n = 6-13$ ).  $*p < 0.001$  compared to wild-type CLH-3b.  $^{\ddagger}p < 0.001$  compared to CLH-3b(E167C).

time constants for CLH-3b(E167C) $\Delta$ 833-1001 and CLH-3b(E167C) $\Delta$ 604-614 were 38 s and 28 s, respectively (Fig. 9 C). Both values were significantly ( $p < 0.001$ ) lower than the MTSET inhibition time constant of 144 s for CLH-3b(E167C). These results indicate that primary structural changes in the CLH-3b cytoplasmic C-terminus that alter channel gating also alter the reactivity of cysteine residues on the extracellular surface of the channel.

## DISCUSSION

Dutzler and co-workers demonstrated that amino acids on helices D, F, N, and R form the selectivity filter and fast protopore gating mechanism in the outer pore vestibule of CIC proteins (4,5) (Fig. 1). The connection of the R helix to large cytoplasmic C-termini in eukaryotic CIC proteins has suggested that these domains may secondarily alter the structure of the outer pore and lead to changes in channel gating and functional properties. Consistent with this idea, Hebeisen and Fahlke (25) have shown recently that truncation of the C-terminus of CIC-1 alters anion binding affinities and the MTSET reactivity of an engineered cysteine residue on helix F.

We suggested previously that C-terminal splice variation of CLH-3a and CLH-3b gives rise to the distinct voltage-dependent gating properties and extracellular  $\text{Cl}^-$  and  $\text{H}^+$  sensitivities of these two channels (14). This hypothesis is supported clearly by the current studies. Deletion of the 169 amino acid C-terminal splice insert unique to CLH-3b (Fig. 1 B) induces functional properties that are identical to those of wild-type CLH-3a (Figs. 2, 3, 6, and 7). Interestingly, the same channel properties are induced by deletion of the last 11 amino acids of CBS1 (Figs. 6 and 7). These results suggest that a functional interaction exists between CBS1 and the distal C-terminus of the channel. This functional interaction could be mediated by a direct interaction between the two protein domains. Alternatively, both domains may be necessary for maintaining secondary and tertiary structure that modulates overall channel properties.

The glutamate gate plays a central role in voltage,  $\text{Cl}^-$ , and  $\text{H}^+$ -dependent gating of CIC channels (4,19,20,24). We postulated that the differences in CLH-3a and CLH-3b voltage,  $\text{Cl}^-$ , and  $\text{H}^+$  sensitivity may be due to difference in the conformation of the glutamate gate and selectivity filter (14). Consistent with this idea, as well as other studies (4,19, 20), mutation of the glutamate gates to alanine gives rise to constitutively active channels that are largely insensitive to changes in voltage and extracellular  $\text{Cl}^-$  and  $\text{H}^+$  (Fig. 8).

We performed cysteine mutagenesis experiments to begin characterizing the effect of C-terminal splice variation on the conformation of the extracellular surface of the channel. Wild-type CLH-3a and CLH-3b are inhibited 40%–50% by 1 mM MTSET (Fig. 9, A and C). The extent of inhibition and the inhibition time constants are similar for CLH-3a and CLH-3b, suggesting that endogenous extracellular cysteine residues on the two channels have similar MTSET reactivity.

Mutation of the glutamate gates to cysteine increased the extent of MTSET inhibition significantly in both CLH-3a(E238C) and CLH-3b(E167C) (Fig. 9 A). Cysteine mutagenesis had no effect on the CLH-3a(E238C) MTSET inhibition time constant, but it slowed the rate of CLH-3b(E167C) MTSET inhibition by approximately sevenfold (Fig. 9 C). This dramatically slowed MTSET inhibition was nearly fully reversed in the CLH-3b(E167C) $\Delta$ 833-1001 and CLH-3b(E167C) $\Delta$ 604-614 mutant channels (Fig. 9 C). As shown in Figs. 6 and 7, deletion of amino acids 833–1001 and 604–614 in CLH-3b gives rise to CLH-3a-like voltage,  $\text{Cl}^-$ , and pH sensitivity. Our data thus demonstrate that changes in the primary structure of the CLH-3b cytoplasmic C-terminus that alter channel gating also cause conformational changes at the extracellular surface of the channel. These conformational changes in turn alter the MTSET reactivity of extracellular cysteine residues.

It is tempting to speculate that the slowed MTSET inhibition of CLH-3b(E167C) is due to reduced MTSET reactivity of the engineered cysteine residue compared to CLH-3a(E238C) and that the reactivity of this residue is modulated by the structure of the cytoplasmic C-terminus. However, it should be stressed that the actual cysteine residues targeted by MTSET in CLH-3b(E167C) are uncertain. It is conceivable that the E167C mutation slows MTSET inhibition by secondarily altering the reactivity of endogenous extracellular cysteine residues. More detailed structural analysis of the glutamate gate and outer pore structure will require the engineering of a functional cysteineless CLH-3b mutant.

Deletion of the CLH-3b 101 amino acid splice insert (i.e., amino acids 668–768) located between CBS1 and CBS2 (Fig. 1 B) does not alter  $\text{Cl}^-$  or  $\text{H}^+$  sensitivity or induce sensitivity to depolarizing voltages (Figs. 6, A and B, and 7, D and E). Instead, deletion of this splice insert shifts the activation voltage of CLH-3b from  $-32$  mV (Fig. 3 D; (17)) to  $\sim -70$  mV (Fig. 7 B). This deletion also alters the kinetics of hyperpolarization-induced current activation. Hyperpolarization-induced activation of wild-type CLH-3b expressed alone in HEK293 cells is described by fast and slow time constants of  $\sim 5$  ms and  $\sim 135$  ms (Fig. 7 C and Results). Similar fast and slow time constants also describe activation of CLH-3b( $\Delta$ 833-1001) and CLH-3b( $\Delta$ 604-614) (data not shown). In contrast, CLH-3b( $\Delta$ 668-768) activation is described by a single slow time constant (Fig. 7 C and Results).

The effects of deleting the splice insert between CBS1 and CBS2 are remarkably similar to the effects of the Ste20 kinase GCK-3 on wild-type CLH-3b activity. When expressed alone in HEK293 cells, CLH-3b is largely constitutively active. GCK-3 inhibits CLH-3b *in vivo* and in heterologous expression systems by phosphorylating the channel and/or associated regulatory proteins. When coexpressed with the channel, GCK-3 reduces whole cell current levels and shifts the activation voltage from  $\sim -30$  mV to  $\sim -70$  mV. In addition, hyperpolarization-induced activation of the GCK-3-inhibited current is described by a single slow time

constant (17). We suggested previously that GCK-3 may function to inhibit protopore fast gating via signaling events occurring at the cytoplasmic C-terminus (17).

GCK-3 is a homolog of mammalian PASK (proline- and alanine-rich Ste20-related kinase) (26) and binds to the CLH-3b C-terminus via the PASK binding motif RFLI (17). This binding motif is located at the beginning (i.e., R-668–I-671) of the 101 amino acid splice insert. Mutation of phenylalanine at position 669 to alanine prevents GCK-3 binding and channel inhibition (17).

The specific binding of GCK-3 to the 101 amino acid splice insert and the effects of deletion of these amino acids on channel functional properties suggest the intriguing possibility that this splice insert is a regulatory domain. A simple hypothesis to explain our results is that the 101 amino acid domain interacts with another region of CLH-3b. This interaction in turn induces a conformational change that allows channel activation at relatively depolarized membrane voltages. Disruption of this interaction by GCK-3-mediated phosphorylation events or by deletion of the putative regulatory domain converts the channel into an inactive conformation. Additional studies are required to test this hypothesis and to determine how phosphorylation alters channel gating properties and structure.

To conclude, we have shown that splice variation of the cytoplasmic C-terminus accounts for the striking differences in voltage,  $\text{Cl}^-$ , and  $\text{H}^+$  sensitivity of CLH-3a and CLH-3b and that it alters the conformation of the extracellular surface of the channels. Differences in outer pore structure and conformation of the glutamate gates may give rise to differences in CLH-3a and CLH-3b gating. We suggest that the 169 amino acid C-terminal splice insert in CLH-3b represents a “gating module” that modifies the voltage-dependent gating properties of the channel. The 101 amino acid splice insert between CBS1 and CBS2 may be a “regulatory module” that confers phosphorylation-dependent channel regulation (Fig. 1 B). It is interesting to speculate that mutational changes in the cytoplasmic C-terminus represent a major driving force in the evolutionary diversification of eukaryotic CIC channels.

This work was supported by National Institutes of Health grants R01 HL80810 to K.N. and DK51610 to K.S.

## REFERENCES

- Jentsch, T. J., K. Steinmeyer, and G. Schwarz. 1990. Primary structure of *Torpedo marmorata* chloride channel isolated by expression cloning in *Xenopus* oocytes. *Nature*. 348:510–514.
- Jentsch, T. J., M. Poet, J. C. Fuhrmann, and A. A. Zdebik. 2005. Physiological functions of CLC  $\text{Cl}^-$  channels gleaned from human genetic disease and mouse models. *Annu. Rev. Physiol.* 67: 779–807.
- Jentsch, T. J., V. Stein, F. Weinreich, and A. A. Zdebik. 2002. Molecular structure and physiological function of chloride channels. *Physiol. Rev.* 82:503–568.
- Dutzler, R., E. B. Campbell, and R. MacKinnon. 2003. Gating the selectivity filter in CIC chloride channels. *Science*. 300:108–112.
- Dutzler, R., E. B. Campbell, M. Cadene, B. T. Chait, and R. MacKinnon. 2002. X-ray structure of a CIC chloride channel at 3.0 Å reveals the molecular basis of anion selectivity. *Nature*. 415:287–294.
- Miller, C. 1982. Open-state substructure of single chloride channels from *Torpedo* electroplax. *Philos. Trans. R. Soc. Lond. B Biol. Sci.* 299:401–411.
- Miller, C., and M. M. White. 1984. Dimeric structure of single chloride channels from *Torpedo* electroplax. *Proc. Natl. Acad. Sci. USA*. 81:2772–2775.
- Estevez, R., B. C. Schroeder, A. Accardi, T. J. Jentsch, and M. Pusch. 2003. Conservation of chloride channel structure revealed by an inhibitor binding site in CIC-1. *Neuron*. 38:47–59.
- Engh, A. M., and M. Maduke. 2005. Cysteine accessibility in CIC-0 supports conservation of the CIC intracellular vestibule. *J. Gen. Physiol.* 125:601–617.
- Lin, C. W., and T. Y. Chen. 2003. Probing the pore of CIC-0 by substituted cysteine accessibility method using methane thiosulfonate reagents. *J. Gen. Physiol.* 122:147–159.
- Ignoul, S., and J. Eggermont. 2005. CBS domains: structure, function, and pathology in human proteins. *Am. J. Physiol.* 289:C1369–C1378.
- Schriever, A. M., T. Friedrich, M. Pusch, and T. J. Jentsch. 1999. CLC chloride channels in *Caenorhabditis elegans*. *J. Biol. Chem.* 274: 34238–34244.
- Nehrke, K., T. Begenisich, J. Pilato, and J. E. Melvin. 2000. *C. elegans* CIC-type chloride channels: novel variants and functional expression. *Am. J. Physiol.* 279:C2052–C2066.
- Denton, J., K. Nehrke, E. Rutledge, R. Morrison, and K. Strange. 2004. Alternative splicing of N- and C-termini of a *C. elegans* CIC channel alters gating and sensitivity to external  $\text{Cl}^-$  and  $\text{H}^+$ . *J. Physiol.* 555:97–114.
- Rutledge, E., J. Denton, and K. Strange. 2002. Cell cycle- and swelling-induced activation of a *C. elegans* CIC channel is mediated by CeGLC-7 $\alpha/\beta$  phosphatases. *J. Cell Biol.* 158:435–444.
- Rutledge, E., L. Bianchi, M. Christensen, C. Boehmer, R. Morrison, A. Broslat, A. M. Beld, A. George, D. Greenstein, and K. Strange. 2001. CLH-3, a CIC-2 anion channel ortholog activated during meiotic maturation in *C. elegans* oocytes. *Curr. Biol.* 11:161–170.
- Denton, J., K. Nehrke, X. Yin, R. Morrison, and K. Strange. 2005. GCK-3, a newly identified Ste20 kinase, binds to and regulates the activity of a cell cycle-dependent CIC anion channel. *J. Gen. Physiol.* 125:113–125.
- Yin, X., N. J. Gower, H. A. Baylis, and K. Strange. 2004. Inositol 1,4,5-trisphosphate signaling regulates rhythmic contractile activity of smooth muscle-like sheath cells in the nematode *Caenorhabditis elegans*. *Mol. Biol. Cell.* 15:3938–3949.
- Niemeyer, M. I., L. P. Cid, L. Zuniga, M. Catalan, and F. V. Sepulveda. 2003. A conserved pore-lining glutamate as a voltage- and chloride-dependent gate in the CIC-2 chloride channel. *J. Physiol.* 553:873–879.
- Traverso, S., L. Elia, and M. Pusch. 2003. Gating competence of constitutively open CLC-0 mutants revealed by the interaction with a small organic inhibitor. *J. Gen. Physiol.* 122:295–306.
- Denton, J., K. Nehrke, X. Yin, A. Beld, and K. Strange. 2006. Altered gating and regulation of a carboxy-terminus CIC channel mutant expressed in the *C. elegans* oocyte. *Am. J. Physiol.* 290:C1109–C1118.
- Estevez, R., M. Pusch, C. Ferrer-Costa, M. Orozco, and T. J. Jentsch. 2004. Functional and structural conservation of CBS domains from CLC chloride channels. *J. Physiol.* 557:363–378.
- Saviane, C., F. Conti, and M. Pusch. 1999. The muscle chloride channel CIC-1 has a double-barreled appearance that is differentially affected in dominant and recessive myotonia. *J. Gen. Physiol.* 113:457–468.
- Bisset, D., B. Corry, and S. H. Chung. 2005. The fast gating mechanism in CIC-0 channels. *Biophys. J.* 89:179–186.
- Hebeisen, S., and C. Fahlke. 2005. Carboxy-terminal truncations modify the outer pore vestibule of muscle chloride channels. *Biophys. J.* 89: 1710–1720.
- Dan, I., N. M. Watanabe, and A. Kusumi. 2001. The Ste20 group kinases as regulators of MAP kinase cascades. *Trends Cell Biol.* 11:220–230.